HAL
open science

Parametrical Investigation of Transverse Injection in a Dual-Bell Nozzle During Altitude-Varying Conditions

Brian Legros, Luc Leger, Azeddine Kourta, Amer Chpoun, Mohamed Sellam

To cite this version:

Brian Legros, Luc Leger, Azeddine Kourta, Amer Chpoun, Mohamed Sellam. Parametrical Investigation of Transverse Injection in a Dual-Bell Nozzle During Altitude-Varying Conditions. Journal of Propulsion and Power, 2023, 39 (6), pp.875-885. 10.2514/1.B39077 . hal-04265352

HAL Id: hal-04265352

https://hal.science/hal-04265352

Submitted on 30 Oct 2023

HAL is a multi-disciplinary open access archive for the deposit and dissemination of scientific research documents, whether they are published or not. The documents may come from teaching and research institutions in France or abroad, or from public or private research centers.

L'archive ouverte pluridisciplinaire **HAL**, est destinée au dépôt et à la diffusion de documents scientifiques de niveau recherche, publiés ou non, émanant des établissements d'enseignement et de recherche français ou étrangers, des laboratoires publics ou privés.

Parametrical investigation of secondary fluidic injection in a dual-bell nozzle during altitude varying conditions

Brian Legros[1]
University of Orléans, INSA-CVL, PRISME, Orléans, 45100, France,
& National Centre for Scientific Research CNRS – Institute ICARE, Orléans, 45100, France,

Luc Leger[2]
University of Orléans, University Institute of Technology, Orléans, 45100, France,
& National Centre for Scientific Research CNRS – Institute ICARE, Orléans, 45100, France,

Azeddine Kourta[3]
University of Orléans, INSA-CVL, PRISME, Orléans, 45100, France,

Amer Chpoun[4] and Mohamed Sellam[5]
LMEE, University of Evry, University of Paris-Saclay, Evry, 91020, France

Dual-bell nozzle (DBN) is a rocket nozzle concept that could provide a substantial payload gain. The present paper focuses on the impact of radial secondary injection on DBN behaviour during its ascent and descent in the atmosphere. The influence of the secondary injection settling chamber (cavity) volume is discussed. The positive influence of the cavity volume on the DBN behaviour during transition phases has been exposed, and its effects during retransition were shown to be negligible. The use of secondary injection allowed the transition nozzle pressure ratio to be increased by nearly 24% and the lateral forces were reduced to less than 1% of the nozzle thrust. A first approach regarding secondary injection optimisation is finally proposed.

[1] PhD Student, Department of Fluid, Energetics, Combustion and Propulsion (PRISME) & Department of Propulsive Nozzle (ICARE), brian.legros@cnrs-orleans.fr.
[2] Assistant Professor, Department of Propulsive Nozzle (ICARE), luc.leger@cnrs-orleans.fr.
[3] Professor, Department of Fluid, Energetics, Combustion and Propulsion.
[4] Professor, Department Fluid Mechanics and Environment.
[5] Assistant Professor, Department Fluid Mechanics and Environment.

I. Introduction

Nowadays, operating cost reduction and launchers efficiency enhancement have become crucial to reduce the cost of access to space for companies and state agencies. The rising number of competitors in the aerospace industry have triggered well-off companies to decrease their service fees. Today's launchers such as Ariane 5 are using parallel staging which requires the first stage engine to be started before the lift off for reliability reasons [1]. As a consequence, the main stage engine faces off-design operating conditions during the rocket ascent, which induces high losses. As the nozzle geometry is fixed, the ambient pressure variation during the launcher's ascent requires the flow inside the nozzle to be adapted for only one specific altitude. During the launcher's ascent, the nozzle can experience three distinct flow conditions: overexpansion, adapted flow, and underexpansion (see Fig. 1). In order to prevent flow separation inside rocket nozzles which gives rise to flow instabilities and high variable side-loads at low altitudes, the exit area has to be reduced, even if it implies lower performances at high altitude.

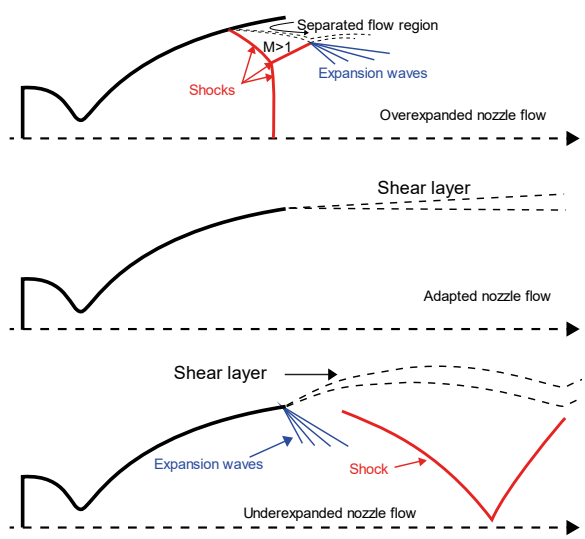

Fig. 1: Conventional bell nozzle working modes. Inspired by [2]**.**

The perfect nozzle would consist of a consistently increasing exit area to adapt to the varying pressure in the atmosphere during the ascent. However, this solution would considerably increase the complexity and reliability of the nozzle. Numerous nozzle concepts with altitude adaptive capabilities have been investigated in the past and this paper focuses solely on the dual-bell nozzle.

The dual-bell nozzle (DBN) concept, which was first mentioned by Swan [3], consists of a converging/diverging

nozzle, with a divergent section composed of two successive nozzle profiles of different expansion ratios: a small expansion ratio nozzle (base nozzle) to provide better performance at low altitude with little risks of side-loads, and a larger expansion ratio nozzle (extension nozzle) for better vacuum performance. The DBN geometry is illustrated in Fig. 2.

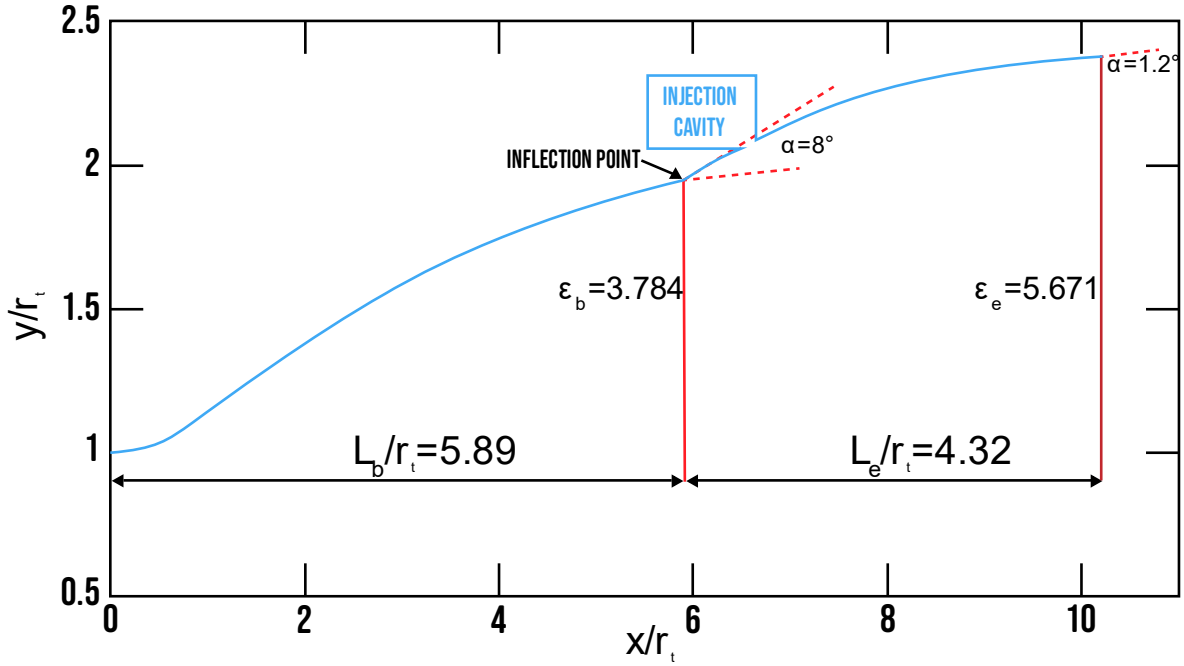

Fig. 2: Geometrical parameters of the DBN profile used during the test campaign.

The two bell profiles forming the divergent section are linked together through an inflection section. During sea-level mode, the flow separates from the nozzle wall at the inflection point, providing a controlled, symmetric flow separation and thus limiting the risks of side-loads. As the launcher ascends into the atmosphere, the ambient pressure decreases and the flow will suddenly reattach in the extension nozzle, shifting the separation location at the nozzle exit, and providing better vacuum performance at high altitudes.

Fig. 3 shows schlieren images of the DBN in low-altitude mode and high-altitude mode during an experiment performed in the wind tunnel described in Sec. II: the low altitude mode, and the high-altitude mode. The high ambient pressure during the low altitude mode forces the flow to separate at the inflection point, which is the onset of the separation shock location (1). The separation shock propagates downstream and it is reflected on the nozzle symmetry

axis. The reflected shock (3) is turned downstream into an expansion fan (4) at the contact of the exhaust plume boundary (2). Then, a series of compression waves merge together downstream to form another recompression shock (5). This process continues downstream, forming a series of compression and expansion cells. In high-altitude mode, the flow is attached to the second bell and an expansion fan (6) exists at the inflection point. The extension profile geometry, which is characterised by a constant pressure profile in Fig. 3, gives rise to an internal recompression shock (7), which directly interacts with the nozzle lip shock (8). The nozzle lip shock intersects with a Mach disc (9) at a triple point as represented on Fig. 3. The reflected shock (3) issued from the triple point is turned into an expansion fan at the jet boundary (2). This process also continues downstream to form a series of compression and expansion cells.

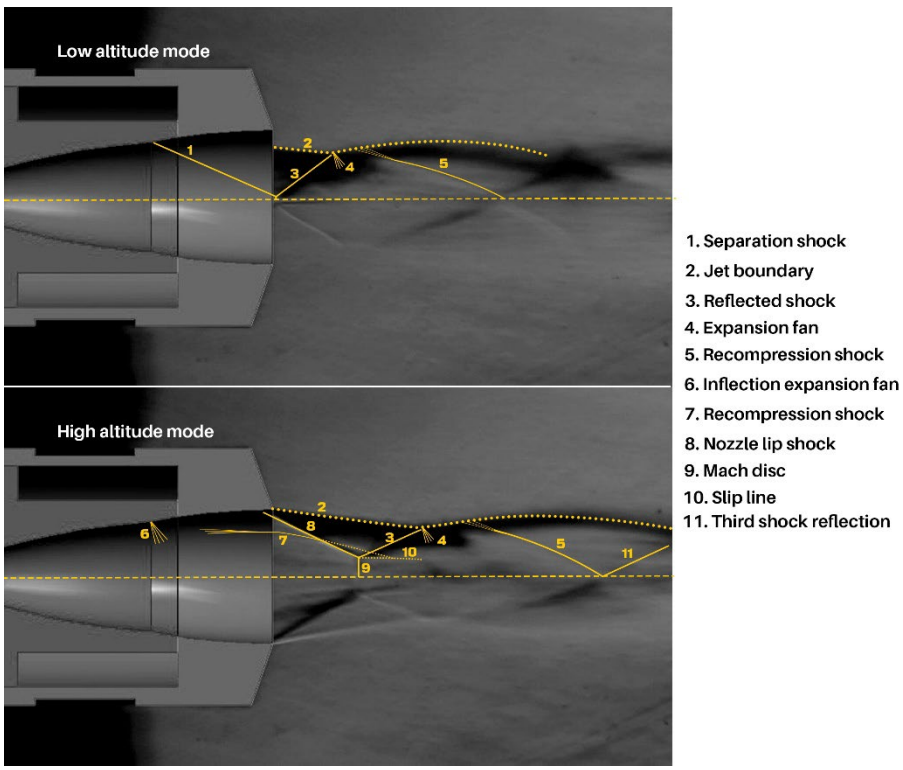

Fig. 3: DBN in low altitude mode (NPR = 15) on the top and high-altitude mode (NPR = 20) on the bottom.

Given the clear potential of dual-bell nozzles to reduce the cost of access to space, they became subject to investigations in many research centers [4–7].

Optimisation codes developed to quantify the financial gain on an Ariane-5-like launcher, with its Vulcain 2 engine

mounted with a dual-bell nozzle, showed a payload mass gain into geostationary transfer orbit of 490 kg [1]. Furthermore, an analysis performed by Ferrero et al. [8] for similar operating conditions indicated a payload mass gain of 1.5 tons using a DBN equipped with an optimised radial secondary injection to control the flow separation during the ascent.

Even though the DBN appears to be promising and easy to implement with no cooling issues, three main issues have to be carefully considered in order to make the DBN a viable concept: 1) Early transition and retransition, 2) Lateral forces generation, 3) Stability.

In the best-case scenario, the transition from low to high altitude mode (and vice versa) must take place as close as possible to the optimum transition point to provide the best performances (see Fig. 4). However, the natural transition and retransition in DBNs take place before the optimum transition point (as seen Fig. 4). Therefore, an efficient method has to be implemented to delay these critical phases. Moreover, the shift from one mode to the other produces undesirable side-loads caused by unsteady and asymmetrical flow separation which could be detrimental to the rocket integrity [9,10].

Transition in DBN depends on several parameters that are still the subject of numerous studies: Reynolds Number, testing environment, nozzle geometry, ambient pressure fluctuations, temperature etc. [10–14].

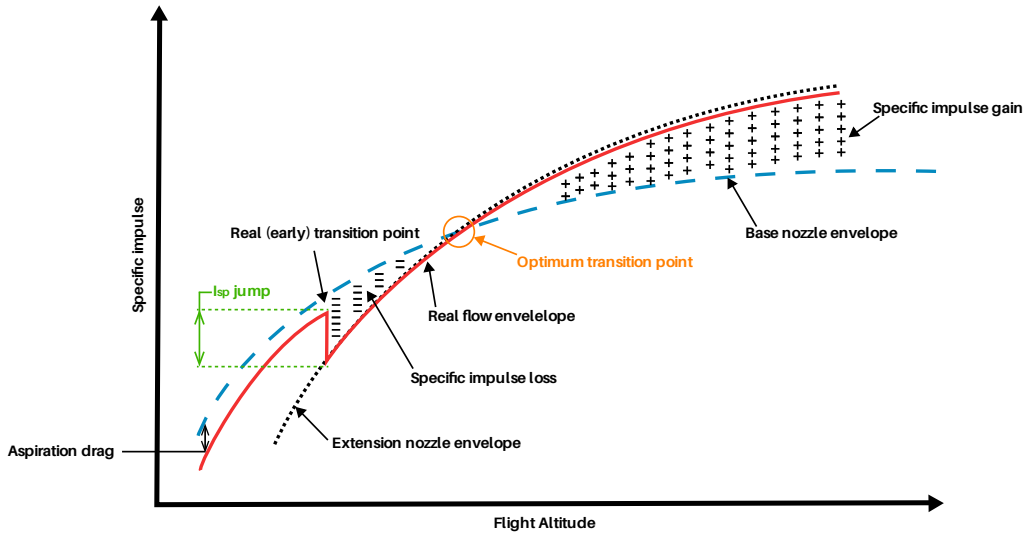

Fig. 4: DBN efficiency compared to conventional nozzles inspired by [2]**.**

The extension contour type is one of the key parameters to control the transition behaviour [15]. There are three

different types of extension profiles: Negative wall Pressure gradient (NP), Positive wall Pressure gradient (PP), and Constant wall Pressure (CP).

In NP extension profiles, separation location was found to be dependent on the nozzle pressure ratio, and was well predicted by flow separation criterion such as the Schmucker's criterion [16]. No sudden transition is observed in NP extension profiles, and the slow movement of the separation front is the cause of important side-loads [5,16].

However, in the case of PP extension profiles and CP extension profiles, a sudden transition is observed experimentally [5,16] and numerically [17], thus, reducing the risks of side-loads generation [5,16,18].

The extension length also plays an important role on the performances of DBNs. Decreasing its length would decrease the lever arm, and consequently reduce the magnitude of the side-loads. However, decreasing the extension length also reduces the stability of the DBN with a smaller hysteresis [10], where the hysteresis is defined by the difference between the transition NPR and the retransition NPR.

Extreme caution should be taken during DBN wind tunnel testing, as many studies demonstrated that DBNs behaved differently depending on whether the tests were performed in altitude chambers or at ambient conditions. Varying the feeding total pressure during experiments also greatly influences the behaviour of DBNs as it changes the Reynolds number and modifies the effective wall shape of the sensitive inflection region [11,15,19–21]. Though many of the previous studies provided significant information on DBN behaviour during the ascent and descent phases, only a few of them have focused on the control of transition and retransition, as well as side-loads generation in DBNs.

Flow control in rocket nozzles has been the subject of numerous studies, whether to prevent flow separation in overexpanded nozzles at low altitude, to control thrust vector, or to decrease side-loads amplitude on a launching pad [22,23]. Flow control in dual-bell nozzles has been mainly investigated by using film cooling and secondary injection normal to the mainstream direction, principally to control the transition.

Film cooling in the vicinity of the inflection region showed a decrease in transition NPR in [24], but an increase in [25]. A reduction of thrust jump in the transition phases, and lower side-loads (an example of thrust jump is shown in Fig. 4) were also reported. In [26], an effective capability of lowering the wall temperature at the cost of long-lasting lateral forces capable of exciting a nozzle structural mode was indicated.

In the case of radial secondary fluidic injection, significant gains could be found even for relatively small secondary mass flow rate. Indeed, a small percentage of the mainstream mass flow was sufficient for the secondary injection to increase the transition nozzle pressure ratio [27] when the injection was located downstream of the inflection point.

As the ambient pressure starts to decrease and the transition from low-to-high altitude mode tends to happen, the radial injection of secondary fluid acts as an obstacle to the upstream flow, triggering a forced and symmetrical flow separation in the inflection region. The presence of the injection gives birth to a separation shock, in addition to the regular shock pattern visible in conventional dual-bell nozzle studies. Using the radial secondary injection, the flow will remain detached on a longer NPR range and bring one towards the optimum transition point [12,27]. Furthermore, radial secondary injection also has a positive impact on the nozzle stability and it reduces lateral forces generation as indicated in [28]. Indeed, a decrease in side-loads magnitude to the extent that the force balance could not capture the lateral forces anymore was observed in [28]. Secondary injection was also found to be useful to reduce the flip-flop behaviour of the shock system during the retransition phases, where the flip-flop phenomenon corresponds to a high amplitude and unsteady displacement of the separation point. In this paper, the authors study the influence of the secondary injection cavity volume (see Fig. 6), and the impact of the secondary mass flow rate ratio ($\varphi_{\dot{m}}$, defined in Sec. B) on a subscale dual-bell nozzle behaviour during the ascent and descent phases of a rocket in the atmosphere.

II. Experimental Setup

The experiments were performed in the EDITH depressurized wind tunnel (WT) (see Fig. 5). The test facility was the same as described in [27]. EDITH is one of the rare nozzle testing facility offering nozzle exit pressure variations. Dry air from 320 litre tanks and pressurised at 30000 kPa is regulated to 350 kPa to serve as the nozzle feeding total pressure. Then, the air travels through the dual-bell nozzle and exits in the depressurised WT test section. The pressure inside the test section is controlled by a valve located in the WT diffuser, upstream of an overall 345 kW pumping group. The opening, and closing of this valve allows one to decrease, and increase the pressure inside the WT test section. During the experiments, the dual-bell nozzle is mounted on a force balance designed by the authors and which moves freely along the (x,y,z) orthogonal axis. The thrust and lateral forces are measured by the force balance using four HBM S2 strain-gauge force transducers, whose signals are amplified to a 0-10 V range before being acquired by the SCXI-1140 cards, at the rate of 1 kHz. The HBM S2 is a force sensor with an accuracy class of 0.05 which provides high accuracy measurements. Two transducers of 200 N located on both sides of the force balance were used to measure the vertical force component; one 200 N transducer measured the nozzle thrust; and a 20 N transducer measured the lateral forces. Previous studies for the validation of the force balance measurements showed a 0.24 N standard deviation for the force measurements on the longitudinal axis, 0.06 N on the vertical axis and 0.17 N on the lateral axis.

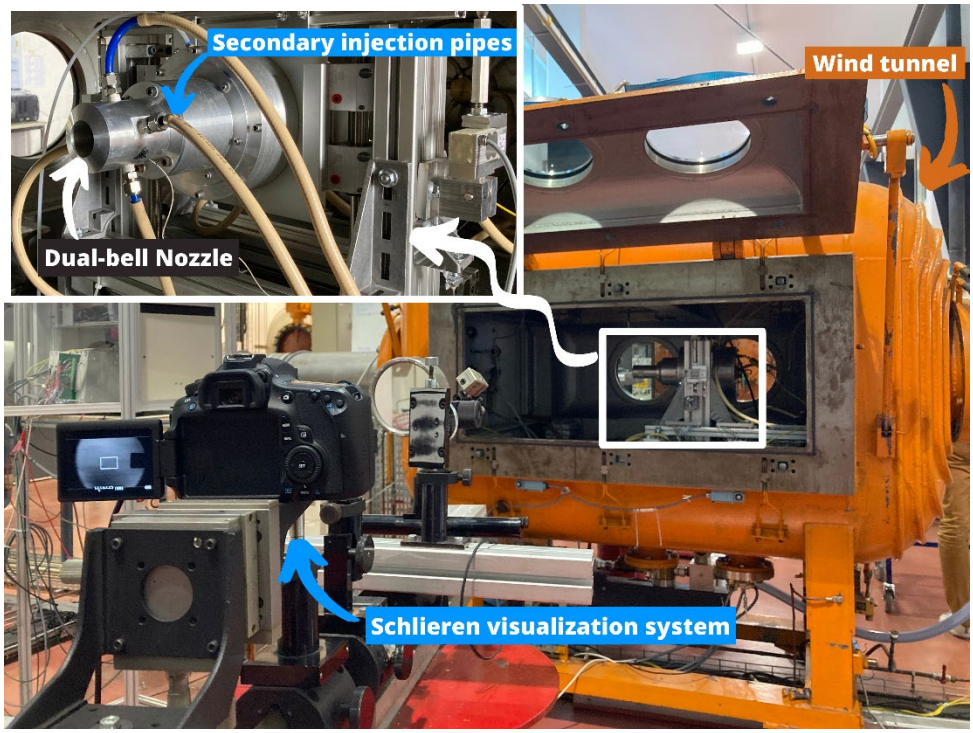

Fig. 5: EDITH wind tunnel testing facility.

The base nozzle was designed as an ideal contour (TIC) for an exit Mach number of 3. At the truncated section, the wall Mach number M_b was 2.76. The extension nozzle was built as a constant pressure (CP) extension profile for a Mach number M_e of 3.17 after the expansion (α=8°). To actively control the flow transition and retransition behaviour, a secondary flow of air was radially injected in the extension part of the DBN. The 0.2 mm width injection slot was made possible by manufacturing the DBN in two parts, and the slot was placed 8 mm downstream of the inflection point. This technique also allowed the creation of a settling chamber for the secondary injection (called cavity, and visible in Fig. 6), to provide an axisymmetric, homogeneous secondary injection. The DBN parameters are summarized in Table 1.

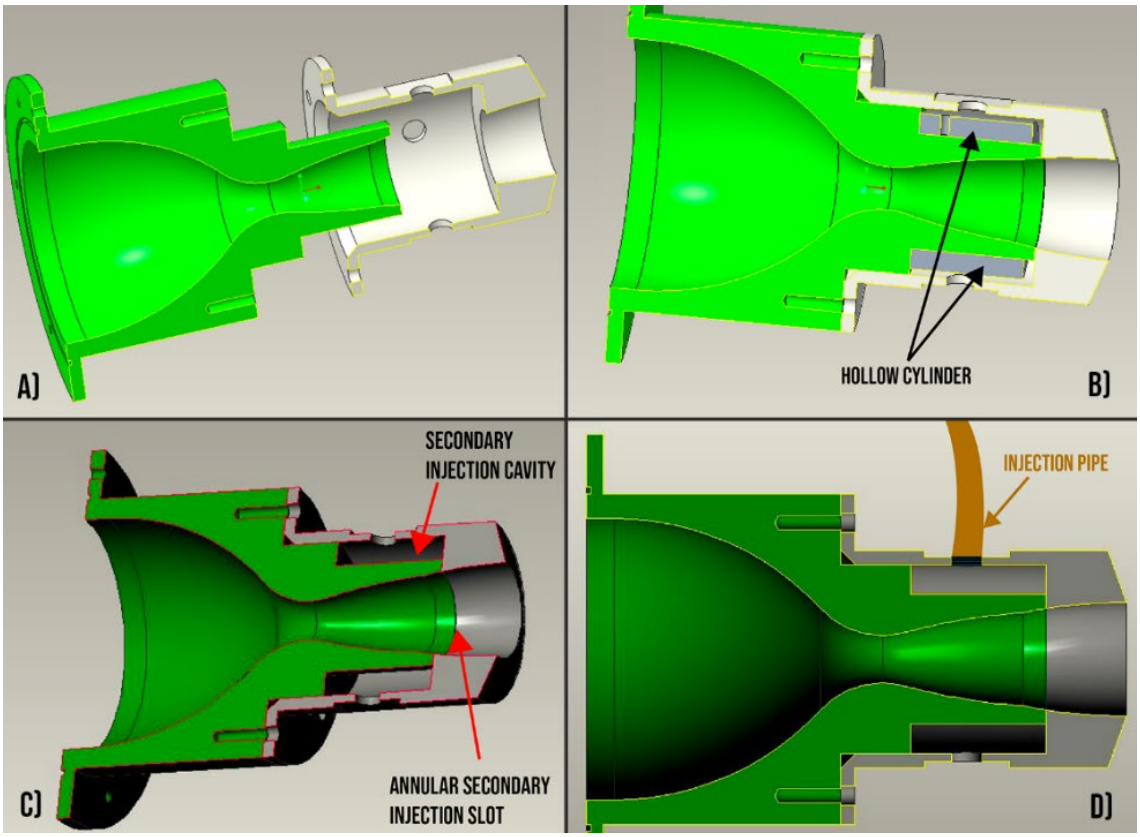

Fig. 6: Disassembled DBN in A). DBN with hollow cylinder configuration in B), with empty cavity in C), with cavity with pipes in D).

In this study, two test campaigns have been carried out. The first one was performed without injecting a secondary fluid as it allowed the authors to investigate the influence of the cavity volume on the DBN transition behaviour. In this campaign, a hollow cylinder was manufactured to be inserted into the cavity in order to provide a smaller secondary injection chamber volume compared to the original cavity. The second test campaign explored the influence of the secondary mass flow rate ratio ($\varphi_{\dot{m}}$) on the subscale DBN transition behaviour. In this case, several secondary injection pressures were used, ranging from 37 kPa to 217 kPa, corresponding to a mass flow rate ratio range of 0.011 to 0.062. Within this range of secondary injection pressures, the secondary jet was sonic at the injection slot exit, except when the secondary injection pressure was set to 37 kPa.

For all experiments, the DBN feeding total pressure was kept constant at 350 kPa and the ambient pressure was varied using the main exit valve located upstream of the pumping group to trigger the transitions and the retransitions in the DBN. When secondary injection was used, the injection pressure was kept constant throughout the experiment. The ambient pressure and the secondary feeding total pressure inside the cavity were measured using Kulite XCQ-062

pressure transducers of 0-100 kPa range. For secondary injection pressures above 88 kPa, the pressure transducer inside the cavity was replaced by a Kulite XCQ-093 of 0-350 kPa range with a sensitivity of 28.743 mV/bar. Geometrical details of the DBN profile obtained by an in-house code based on the method of characteristics are presented in Fig. 2, and the reader can find further details in [27,28]. The nozzle flow visualisation was made possible via the Z-Schlieren system described in [27] and a Canon EOS60D camera, recording images at a frequency of 50 Hz. All-important results obtained in the manuscript are summarised in Table 3.

Table 1: DBN parameters

Throat radius	r_{th} = 0.0085 m
Base nozzle geometry	Length: l_b/r_{th} = 5.89
	Expansion ratio: ϵ_b= 3.78
Extension nozzle geometry	Length: l_{ext}/r_{th} = 4.32
	Expansion ratio: ϵ_{ext}= 5.67
Inflection angle	α = 8°
Injection slot location	8 mm downstream the inflection point
Design transition NPR (Stark separation criterion)	NPR_{trans} = 14.89

III.Results and discussions

A. Cavity effects on dual-bell nozzle behaviour

The secondary injection inside the divergent section of a dual-bell nozzle requires an external cavity to set the stagnation conditions for the secondary jet and to insure a uniform circumferential injection (see Fig. 6). However, the potential effect of the cavity presence has not been investigated yet and reported in the open literature. This section aims to provide an insight of the injection cavity volume effect on transition and retransition behaviour in DBNs. To do so, 4 different experiments were performed in the EDITH depressurized wind tunnel using: 1) A DBN called smooth nozzle without an injection slot; 2) A DBN with an injection slot and an empty cavity; 3) A DBN with an injection slot and a cavity with a hollow cylinder inside in order to decrease its volume; 4) A DBN with an injection slot and an empty cavity connected to the secondary injection pipes, but without an operating secondary injection in order to obtain a larger cavity volume. During the experiments involving the filled cavity and the empty cavity, the holes used for the secondary injection pipes connection were blocked using plugs. The filled cavity, the empty cavity, and the empty cavity connected to the injection pipes had respectively an internal volume of 30.1 cm^3, 89.8 cm^3, and 558.8 cm^3.

For each configuration, the experiments were performed so as to provide an average of fourteen transitions and retransitions phases per configuration, and to allow the calculation of the standard deviation. This important number of data points allows to take into account the total temperature influence during the experiments, caused by the tanks flow expansion from 30000 kPa to 350 kPa to generate the mainstream flow. Fig. 7 shows the evolution of the specific impulse (I_{sp}), NPR and normalized side-loads during a typical run of the wind tunnel for the empty cavity connected to the injection pipes but without an operating secondary injection. The normalized side-loads are obtained by dividing the lateral forces by the thrust in order to be able to analyse the peaks as a percentage of the thrust.

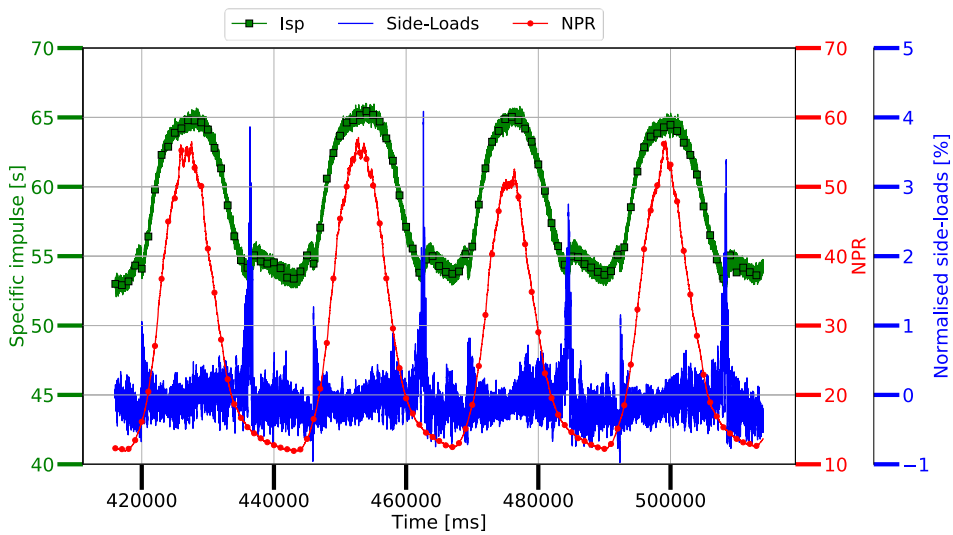

Fig. 7: I_{sp}, NPR, and side-loads as a function of time using a DBN with cavity connected to the injection pipes, but without any secondary injection.

The EDITH wind tunnel happened to offer remarkable operating conditions with consistent repeatability and reliability of the measurements. Below NPR=15, the dual-bell nozzle functions in the low altitude, overexpanded mode, where the separation line is located in the vicinity of the inflection region. As the NPR is increased from its lowest values (red curve in Fig. 7), the specific impulse generated by the nozzle also increases until a sudden drop which occurs at NPR=15.92 as represented by the green curve in Fig. 7. For this NPR, the transition takes place and the separation front moves from the inflection point to the nozzle exit, switching the DBN from low, to high altitude mode. During the transition, the separation front motion, along with its irregular wall pressure distribution for a given streamwise location produces lateral forces, as represented by the blue peaks in Fig. 7. Starting from the high-altitude mode, as

the NPR is reduced, the specific impulse also decreases until NPR=14.82. If the NPR keeps decreasing, a sudden jump in specific impulse is observed at NPR=14.81, arising from the retransition from high to low altitude mode. In this case, the separation front moves back, from the nozzle exit, to the inflection point. Similarly, the separation front motion generates lateral forces, which are higher during retransition than during transition as depicted in Fig. 7.

Once the experiments were carried out for the four cases (smooth, filled cavity, empty cavity, and empty cavity connected to the injection pipes nozzles), the following parameters were investigated to study the effects of the presence of the cavity in the DBN during transitions and retransitions: a) transition NPR; b) maximum side-loads magnitude peak; c) thrust jump magnitude (see thrust jump example in Fig. 4). Fig. 8 shows the transition NPR (NPR_{trans}) and the retransition NPR ($NPR_{retrans}$) for the smooth DBN and the three DBN cavity configurations. It shows that the cavity volume does not significantly impact the $NPR_{retrans}$ when compared to the smooth nozzle. Nevertheless, the presence of the cavity leads to a slightly greater NPR_{trans}, though the difference between the filled cavity, and the empty cavity, is not clearly noticeable. The very small air pocket volume in the filled cavity case also implies that the simple presence of the injection slot is sufficient to delay transition. Indeed, the injection slot seems to act as an obstacle which maintains the separation location fixed during a short time, inducing a slightly greater NPR_{trans}. However, in the case where the injection pipes were mounted on the cavity, a larger increase in NPR_{trans} becomes visible compared to all the other cases and the NPR_{trans} was increased by 7.3% with respect to the smooth nozzle configuration. This result suggests that the air pocket volume inside the cavity plays a role in DBNs transition behaviour, as the emptying of this bigger volume during the ascent could interfere with the flow at the separation location and delay transition. While the $NPR_{retrans}$ remains fairly unchanged between the smooth nozzle, and the two smallest cavity volume configurations, the increase in NPR_{trans} brings the hysteresis from 2.1% for the smooth nozzle, to 4.6% and 4.9% for the filled, and empty cavity, respectively. In the case of cavity with pipes, the $NPR_{retrans}$ is slightly increased, but in less proportion than the NPR_{trans}, bringing the hysteresis to 7%. Therefore, the existence of an injection slot, and the volume of air inside the cavity volume not only grants a delay in transition NPR, but also increases the stability of the DBN.

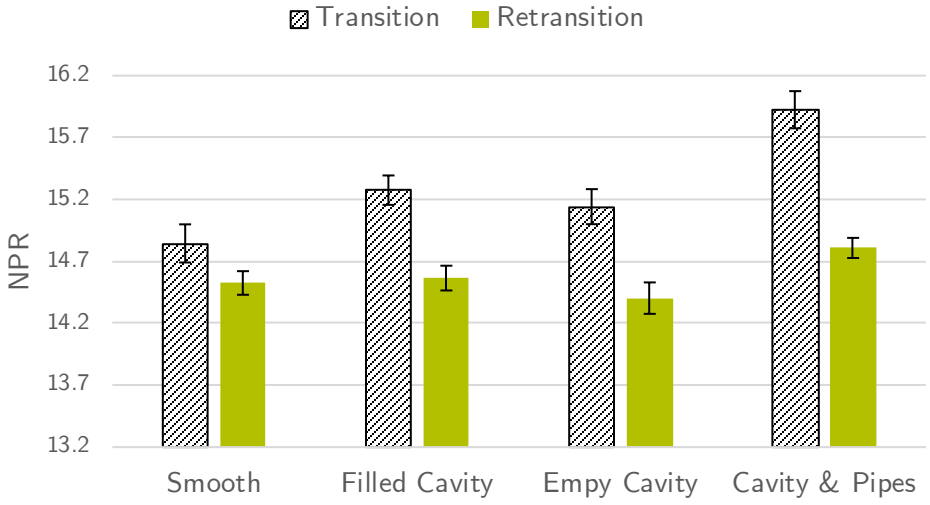

Fig. 8: Transition and retransition NPR for different configurations. Error bars show the standard deviation calculated for each configuration.

Similarly to the previous analysis on retransition NPR, the influence of the cavity volume on side-loads generation during retransition could not clearly be identified in Fig. 9 where the normalized maximum lateral forces during transition and retransition for every configuration is displayed. For the smooth, empty cavity, and cavity with pipes DBN configurations, Fig. 9 shows similar side-loads magnitudes during retransition.

However, the presence of a cavity decreased by more than half the lateral forces generated during transition for the two biggest cavity volume configurations compared to the smooth DBN, with a maximum decrease of 1.3 percentage point in the empty cavity case bringing the lateral forces generated from 2.4% of the nozzle thrust in the smooth configuration to 1.1%. The lateral forces reductions might emanate from the more symmetrical separation line induced by the presence of the injection slot located downstream of the inflection region. Even though the decrease in side-loads with the help of the injection slot and the cavity is clear during the transition process, the impact of the volume of air inside the cavity remains uncertain, especially between the empty cavity and the cavity with pipes.

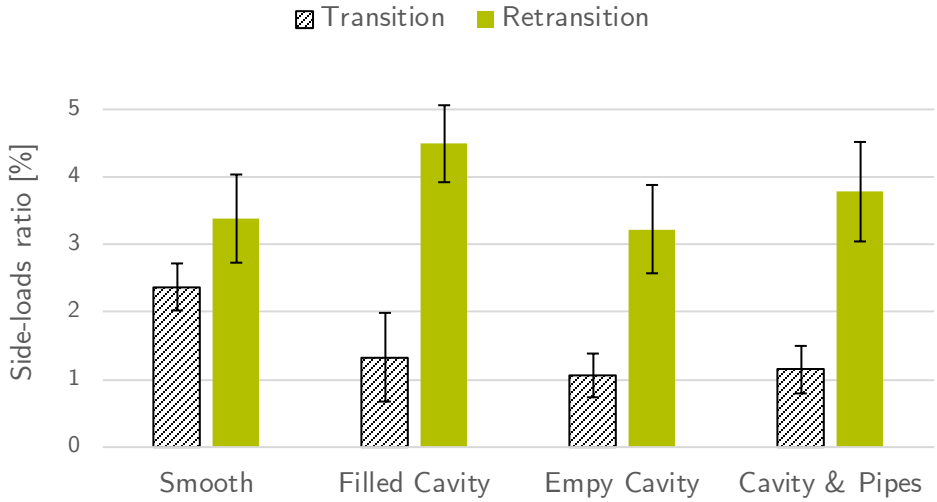

Fig. 9: Lateral forces generated during transition and retransition for different configurations. Error bars show the standard deviation calculated for each configuration.

During the transition and the retransition phases, the motion of the separation front from the inflection region to the nozzle exit (and vice versa) induces a jump in specific impulse (see Fig. 4). The jumps are caused by the sudden change in nozzle area ratio and can be dangerous for the rocket, especially for single-stage-to-orbit (SSTO) vehicles. These sudden variations can be expressed as a jump in specific impulse or, in this study, as a percentage of the nozzle thrust. Fig. 10 shows the normalized thrust jump generated during the transition and the retransition phases for the different configurations. The normalized thrust jump is obtained by dividing the thrust jump by the thrust. The experiments revealed a decrease in both parameters with an increase in cavity volume. During the ascent phase, the thrust jump was reduced by nearly half in the cavity with pipes case compared to the smooth nozzle, dropping from 3.8% of the nozzle thrust to 2.1%. The thrust jump during the descent was decreased in less proportion than during the ascent, as it decreased at best by a fifth, going from 4.2% of the nozzle thrust to 3.4%. The corresponding findings are in accordance with the expected DBN operating behaviour as the presence of the cavity delays the transition NPR, the sudden jump in specific impulse is reduced during the ascent.

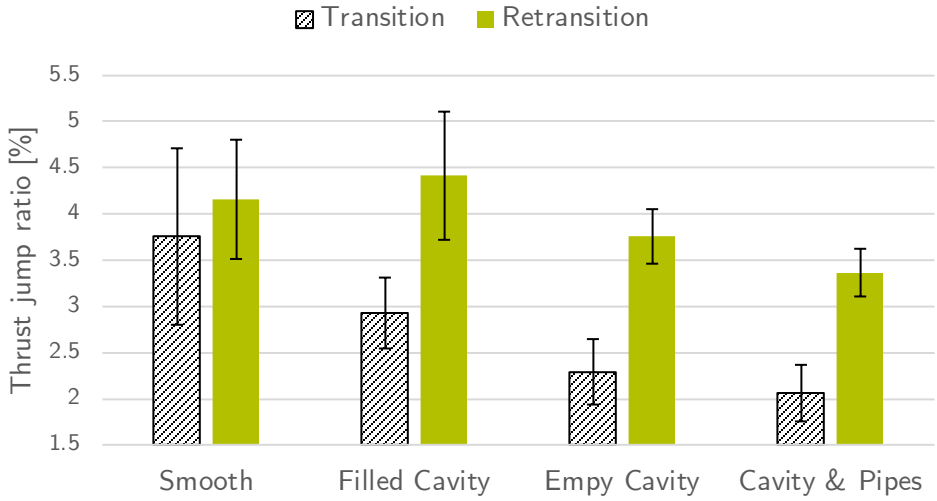

Fig. 10: Thrust jump during transition and retransition for different configurations. Error bars show the standard deviation calculated for each configuration.

B. Secondary injection effects on dual-bell nozzle behaviour

This section consists in analyzing the influence of the secondary injection magnitude on the DBN transition and retransition behaviour. During this test campaign, the total feeding pressure and the secondary injection pressure were kept constant, while the ambient pressure in the wind tunnel was repetitively increased and decreased to trigger the transitions and the retransitions inside the DBN. Several secondary injection pressures were considered for this study. The secondary pressure values (P_i), the secondary pressure ratios ($SPR = \frac{P_i}{P_0}$), the theoretical secondary mass flow rates ($\dot{m}_i$) and the secondary mass flow rate ratios ($\varphi_{\dot{m}} = \frac{\dot{m}_i}{\dot{m}}$) are detailed in Table 2. Here, $\dot{m}$ corresponds to the mainstream mass flow rate of 187 g/s. Fig. 11 shows the evolution of the measured parameters during a typical experiment using $\varphi_{\dot{m}}$ =0.015 (SPR=0.15). The processes of transition and retransition are similar to the ones observed in the cavity influence study, and have already been described in Sec. A.

Table 2: Secondary injection pressure, pressure ratio, mass flow rate, and mass flow rate ratio used in the test campaign

P_i [kPa]	37	51	69	88	126	163	217
SPR	0.11	0.15	0.2	0.25	0.36	0.47	0.62
$\dot{m}_i$ [g/s]	1.98	2.73	3.7	4.72	6.73	8.75	11.63
$\varphi_{\dot{m}}$	0.011	0.015	0.02	0.025	0.036	0.047	0.062

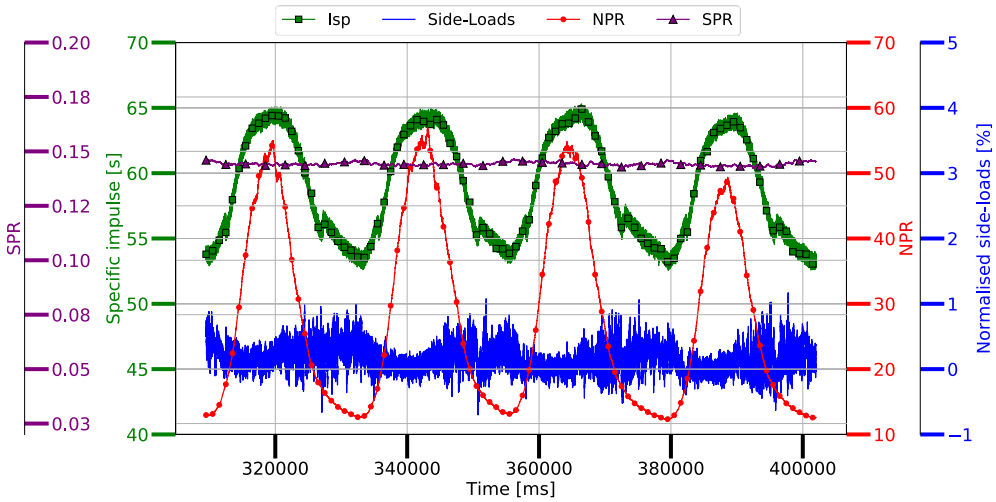

Fig. 11: I_{sp}, NPR, side-loads, and secondary pressure ratio as a function of time during an experiment of DBN with a secondary pressure ratio of 0.15.

Fig. 12 shows the dual-bell nozzle in high altitude mode (NPR=40) for different secondary mass flow rate ratios. It shows that the angle of the shock induced by the secondary injection increases with an increase in secondary mass flow rate ratio to form a Mach disc for the two highest injection cases, though for $\varphi_{\dot{m}}$=0.062, the Mach disc is hidden by the nozzle wall. Indeed, the secondary jet generates a bow shock ahead of the injection and the jet induced adverse pressure gradient triggers the separation of the upstream boundary layer. The shock resulting from the coalescence of the separation shock and the bow shock is reflected on the symmetry axis. The reflected shock interacts with the internal recompression shock due to the constant pressure extension profile. Depending on the secondary mass flow rate, the reflected shock will, or not, hit the exhaust plume boundary and be turned into an expansion fan. Moreover, a significant increase in the exhaust plume diameter is visible for the two highest secondary mass flow rate ratio cases in the vicinity of the shock interaction with the exhaust plume boundary.

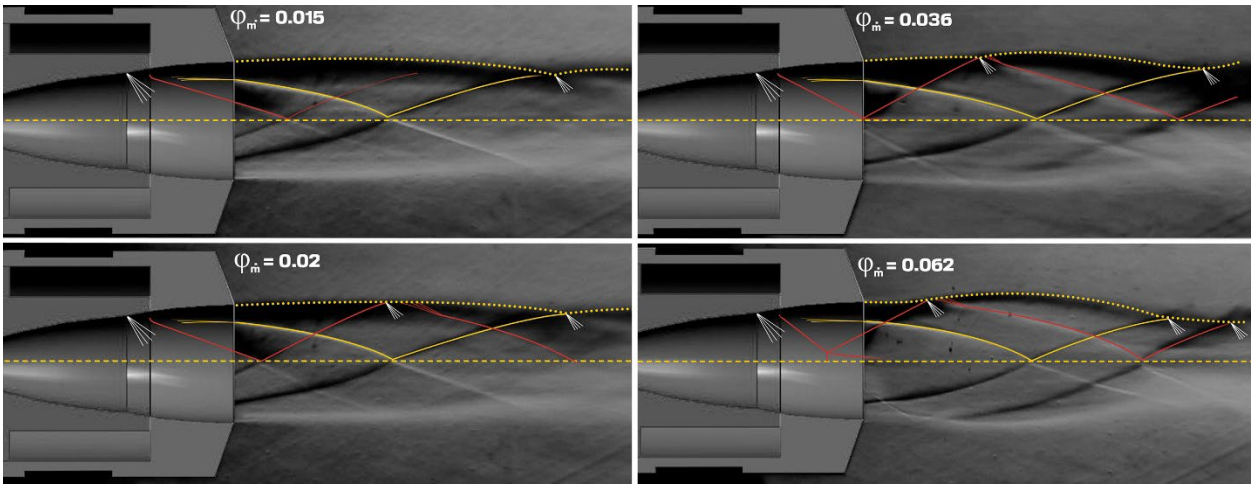

Fig. 12: Schlieren imaging of the DBN for different secondary injection mass flow rate in high altitude mode.

Fig. 13 shows the evolution of the transition and the retransition NPR as a function of secondary mass flow rate ratio. The configuration associated with a mass flow rate ratio of 0 on Fig. 13, Fig. 14, and Fig. 15, corresponds to the case with the empty cavity connected with the injection pipes, but without any injection.

The experiments performed with secondary injection in the extension profile confirm that the NPR_{trans} and $NPR_{retrans}$ are greatly influenced by the secondary injection jet (see Fig. 13). From $\varphi_{\dot{m}}$=0.011 to $\varphi_{\dot{m}}$=0.025, the NPR_{trans} increased when the secondary mass flow rate ratio was increased. The NPR_{trans} rose between a minimum value of 8.2% up to a maximum value of 15.5% compared to the cavity with pipes case, where the transition NPR was 15.92. Similarly, from $\varphi_{\dot{m}}$=0.011 to $\varphi_{\dot{m}}$=0.036, the $NPR_{retrans}$ increased within a range of 13.3% to 17.8% with an increase in secondary mass flow rate ratio, bringing the $NPR_{retrans}$ from 14.81 for the cavity with pipes case, up to 17.45. The transition NPR and the retransition NPR reached a maximum value of 18.39 and 17.45 respectively. The two maximums were reached for a different secondary mass flow rate ratio: $\varphi_{\dot{m}}$=0.025 for the transition phases, and $\varphi_{\dot{m}}$=0.036 for the retransition phases. From the previous maximum values of NPR_{trans} and $NPR_{retrans}$, an increase in secondary mass flow rate ratio induced a decrease in both parameters. In the highest mass flow rate ratio case ($\varphi_{\dot{m}}$=0.062), the decrease in NPR_{trans} and $NPR_{retrans}$ compared to their maximum values reached 5.7% and 0.9% respectively. Fig. 13 clearly shows that there exists a limit in delaying the transitions phases, as there is a point from which an increase in secondary mass flow rate ratio causes a decrease in NPR_{trans} and $NPR_{retrans}$. Using important secondary injection pressures might change the physics involved in the flow; further investigations using computational fluid dynamics should provide explanations to the previous behaviour. Furthermore, it is important to

keep in mind that having the highest transition and retransition NPR does not mean better performances if the secondary mass flow rate necessary to reach these maximums is such that the specific impulses are deteriorated along the flight trajectory.

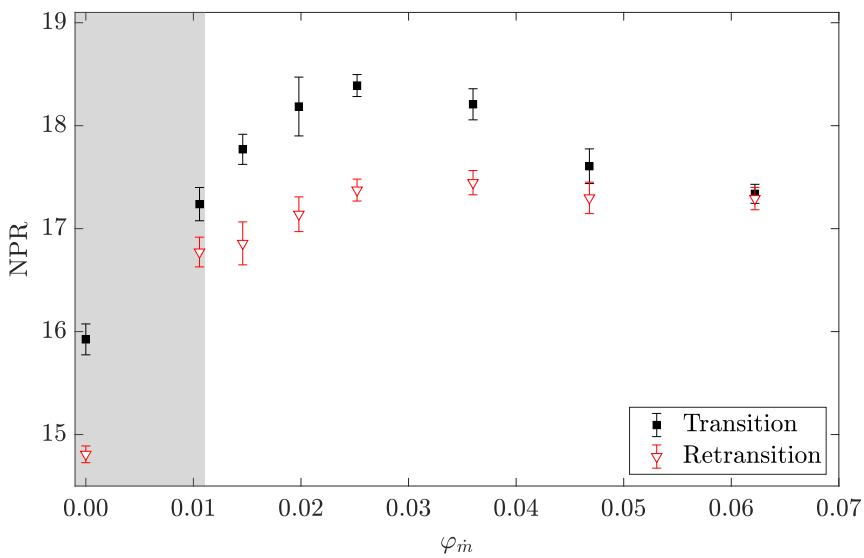

Fig. 13: Transition and retransition NPR versus secondary mass flow rate ratio. Greyout area defines when secondary injection is subsonic. Error bars show the standard deviation calculated for each configuration.

The hysteresis was the largest for the cavity without injection, reaching 7%, then decreased to 2.7% for $\varphi_{\dot{m}}$=0.011, and progressively increased along with the secondary injection pressure to hit a maximum of 5.7% for $\varphi_{\dot{m}}$=0.02. A further increase on secondary mass flow rate ratio induced a decrease in stability as the hysteresis became smaller, dropping to 0.3% for the highest mass flow rate ratio. It is worth reminding that the secondary injection jet was not injected at a sonic speed in the case of $\varphi_{\dot{m}}$=0.011. Therefore, the influence of the subsonic jet may have played a role in the early retransition in this specific case, as the cavity is free to suck or blow air freely in the vicinity of the injection slot region.

By using radial secondary injection in the extension nozzle, the lateral forces generation were considerably reduced (see Fig. 14). From $\varphi_{\dot{m}}$=0.015 and above, the side-loads magnitude generated during the transitions and the retransitions falls within the balance measurement noise ($\pm$ 0.5 N). In the aforementioned mass flow rate ratio range, the force balance could not measure any side-loads peak. The presence of the cavity was already sufficient to decrease

the lateral forces compared to the smooth configuration as the side-loads generated during transitions dropped from 2.4% of the nozzle thrust to 1.1%. Eventually, once secondary injection was used for $\varphi_{\dot{m}}$=0.011 and above, the side-loads during transition dropped below 1% of the nozzle thrust.

Lateral forces generated during the retransition phases have always been greater than during the transition phases in the present DBN study. Indeed, the side-loads generated during retransition reached 3.4% of the nozzle thrust in the smooth nozzle configuration. However, secondary injection application brought side-loads during retransition below 1% of the nozzle thrust for $\varphi_{\dot{m}}$=0.015 and above, providing over three times lower lateral forces magnitude compared to the smooth nozzle configuration.

From $\varphi_{\dot{m}}$=0.036 and above, a slight increase in lateral forces is visible during both, the transition and the retransition phases. This rise in lateral forces also falls within the measurement noise.

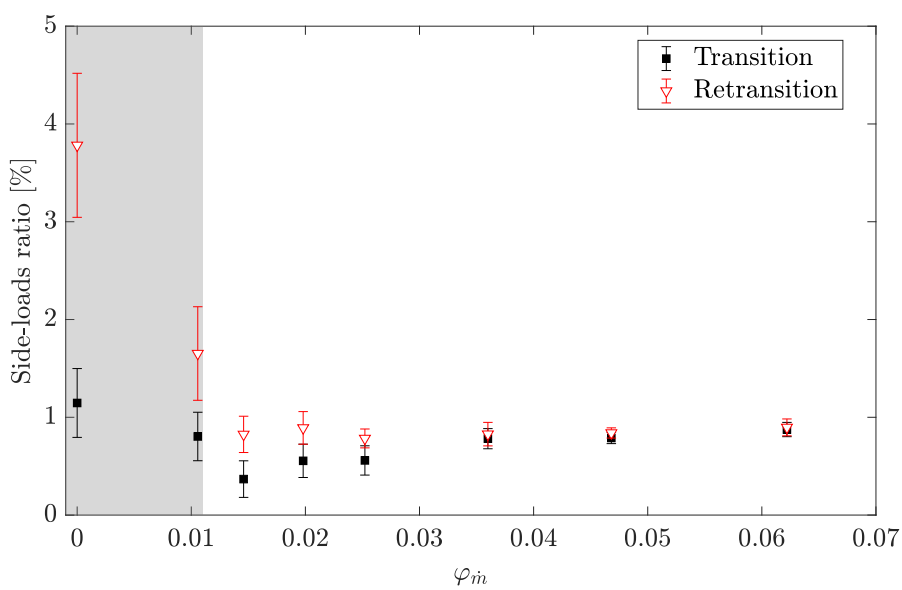

Fig. 14: Lateral forces generated during transitions and retransitions versus secondary mass flow rate ratio. Greyout area defines when secondary injection is subsonic. Error bars show the standard deviation calculated for each configuration.

The influence of secondary injection on thrust jump during the transition and the retransition phases is showed in Fig. 15. The test series revealed that the secondary mass flow rate did not present any significant impact on the thrust jump magnitude during transition and retransition between $\varphi_{\dot{m}}$=0.015 to $\varphi_{\dot{m}}$=0.025 as it stays fairly constant, though much less important than the smooth nozzle configuration. For $\varphi_{\dot{m}}$=0.011, the jumps magnitude during both, the ascent and the descent, are slightly higher than for the other cases. The latter observation might emanate from the non-sonic

secondary injection jet at $\varphi_{\dot{m}}$=0.011 which can be a source of instability in the flow and a more thorough investigation is necessary to validate this hypothesis. Above $\varphi_{\dot{m}}$=0.025, an extra decrease in thrust jump is visible as the secondary injection pressure is increased, though the maximum decrease remains fairly close to the values between $\varphi_{\dot{m}}$=0.015 and $\varphi_{\dot{m}}$=0.025.

However, when comparing the smooth nozzle case to the injection cases, the presence of the injection jet induced a decrease in thrust jump during transition by a factor of 3.2. Fig. 15 also reveals that no significant differences were measured between the cavity connected to the injection pipes configuration and the different injection cases during transition.

Nonetheless, the presence of secondary injection reduced the thrust jump during retransition up to 2.3 percentage points compared to the cavity with pipes case, and 3.1 percentage points (a factor of 3.8) compared to the smooth nozzle configuration. The previous results would be extremely suitable should dual-bell nozzles with secondary injection be used in SSTO launchers. The secondary injection, with its capabilities for decreasing lateral forces and sudden change in nozzle thrust while improving nozzle efficiency, could therefore be seen as a genuine asset for the next generation of reusable launchers.

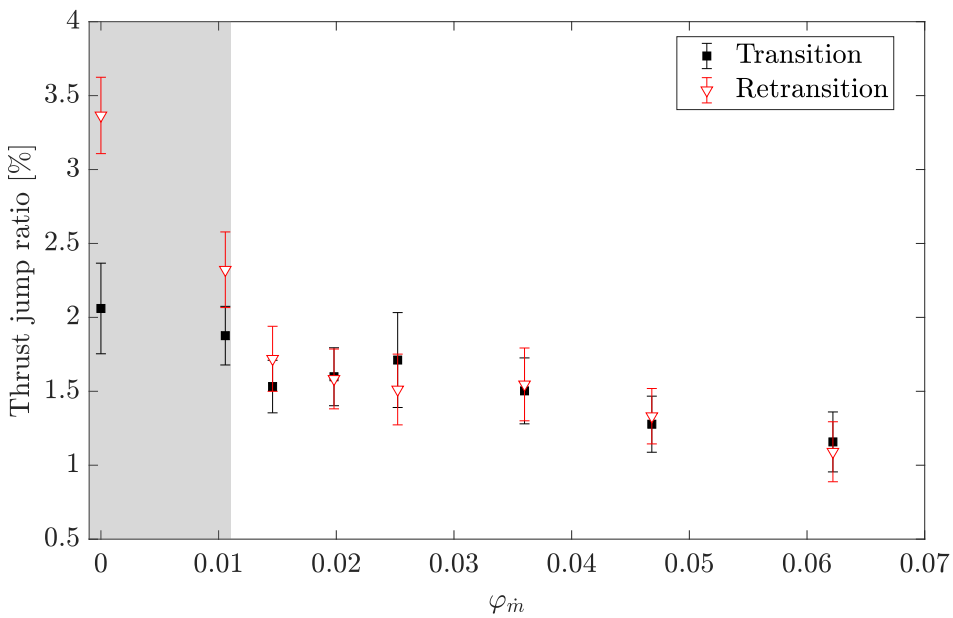

Fig. 15: Thrust jump during transitions and retransitions as a function of secondary mass flow rate ratio. Greyout area defines when secondary injection is subsonic. Error bars show the standard deviation calculated for each configuration.

Fig. 16 shows the theoretical specific impulse of the base nozzle, the extension nozzle, and the experimentally measured specific impulse as a function of nozzle pressure ratio for different secondary mass flow rate ratios during a transition phase. The transition NPR increases with an increase in secondary mass flow rate ratio and then decreases when the secondary jet reaches the maximum value above-mentioned (Fig. 16). Indeed, it highlights the compromise that needs to be achieved between the specific impulse gain obtained from the delayed transition and the losses emanating from the higher secondary mass flow rates injected. Indeed, the increase in secondary injection delays the transition, but the higher the secondary mass flow rate ratio, the greater is the loss in specific impulse.

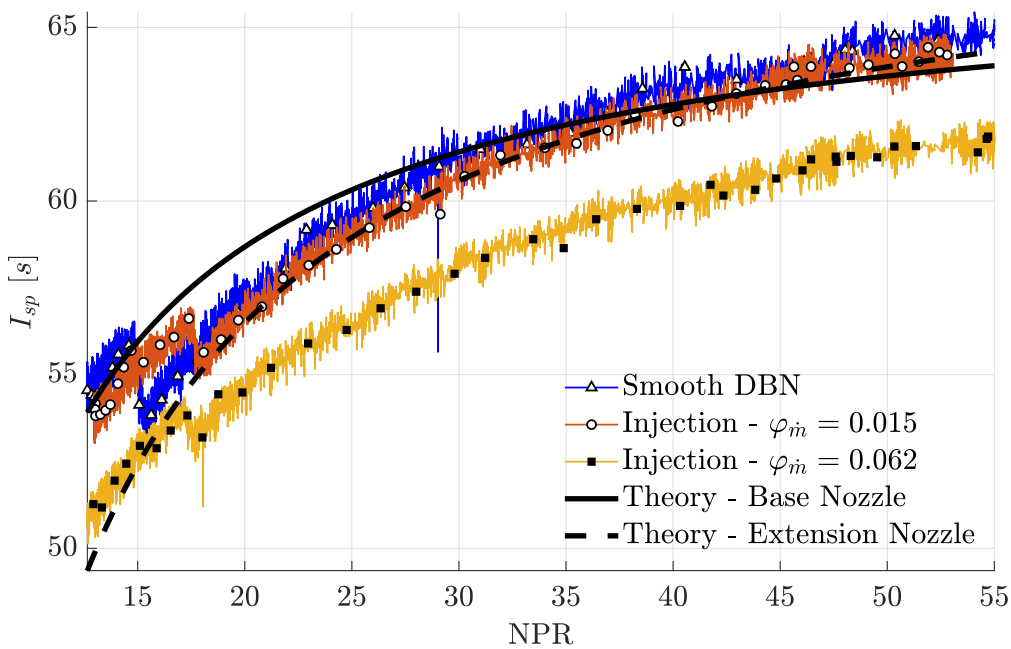

Fig. 16: I_{sp} versus NPR for different configurations. The theoretical performances of the base profile and the extension profile are represented by the black curves.

To determine the best secondary mass flow rate ratio to be used in order to delay the transition NPR while enhancing the performances of the studied DBN, one can define the difference between the specific impulse of the secondary injection cases and the specific impulse of the smooth case:

$$\Delta \mathrm{I}_i = I_{sp_{(inj)_i}} - I_{sp_{(smooth)}} \quad (1)$$

Here, the subscript i refers to the multiple secondary injection configurations.

To compute ΔI_i for each secondary injection configuration, the specific impulse and the NPR during all transition phases of the given configuration were considered (generally fourteen transitions per configuration). From all transition phases of each configuration, an average specific impulse curve $I_{sp} = f(NPR)$ was calculated and used in the equation above.

When ΔI_i is positive, the secondary injection configuration provides better performances than the smooth nozzle configuration after its natural transition NPR. When ΔI_i is negative, the secondary injection configuration provides worse performances than the smooth nozzle configuration. The goal is to determine the secondary injection case where ΔI_i is the greatest.

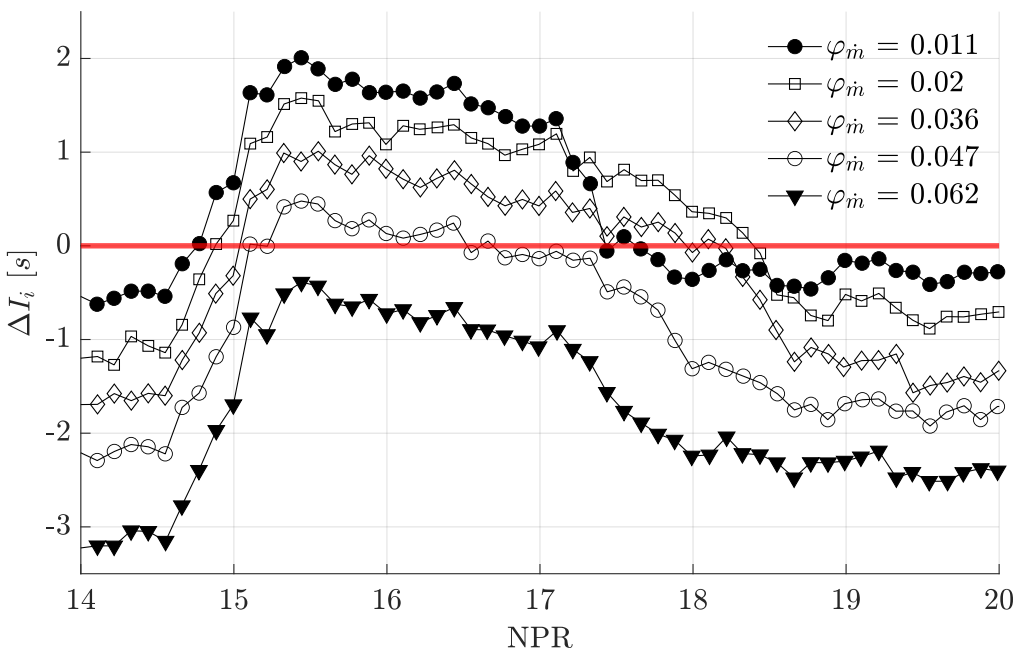

Fig. 17: Specific impulse difference between the smooth DBN configuration and several injection configurations versus NPR.

By comparing the integral of ΔI (when ΔI is positive) for each configuration i, the highest value of ΔI indicates the secondary injection case that provides the best performances. Fig. 17 shows the curve ΔI for the different secondary injection configurations as a function of NPR, where it becomes clear that the transition NPR delay does not balance the specific impulse loss through the highest secondary mass flow rate ratios. Fig. 18 shows the values of the integrals of ΔI as a function of secondary mass flow rate ratio, which gives an indication of the configuration that provides the best performances during the ascent.

In the present case, the secondary mass flow rate ratio that most efficiently delays the transition is close to $\varphi_{\dot{m}}$=0.015. For $\varphi_{\dot{m}}$=0.015, and compared to the smooth nozzle configuration, the use of secondary injection delayed the transition NPR by a fifth while decreasing the thrust jump by 2.2 percentage points. The lateral forces generation were also reduced to less than 1% of the nozzle thrust.

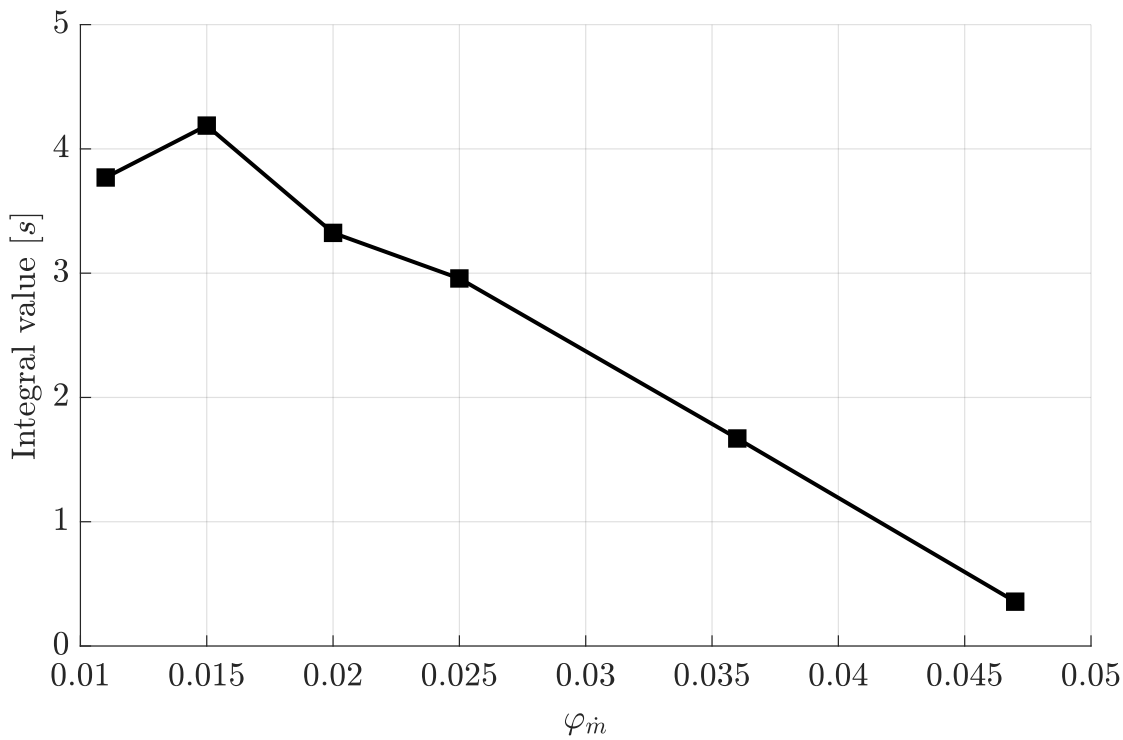

Fig. 18: Integral values of the specific impulse difference as a function of secondary mass flow rate ratio.

Table 3: Summary of the experimental data measured during the test campaign

Configuration	NPR_{trans}	$NPR_{retrans}$	Side-loads ratio$\|_{trans}$ [%]	Side-loads ratio$\|_{retrains}$ [%]	Thrust jump ratio$\|_{trans}$ [%]	Thrust jump ratio$\|_{retrains}$ [%]
Smooth	14.85	14.53	2.37	3.38	3.76	4.16
Filled cavity	15.28	14.57	1.33	4.49	2.93	4.42
Empty cavity	15.14	14.40	1.06	3.23	2.29	3.76
Cavity with pipes	15.92	14.81	1.15	3.78	2.06	3.37
37 kPa	17.24	16.77	0.80	1.65	1.88	2.32
51 kPa	17.77	16.86	0.37	0.83	1.53	1.72
69 kPa	18.19	17.14	0.55	0.89	1.60	1.58
88 kPa	18.39	17.38	0.56	0.78	1.71	1.51
126 kPa	18.21	17.45	0.78	0.83	1.50	1.55
163 kPa	17.61	17.30	0.79	0.84	1.28	1.33
217 kPa	17.34	17.29	0.87	0.90	1.16	1.09

IV. Conclusion and summary of the results

This paper focused on two subjects: the influence of the secondary injection settling chamber volume and the impact of radial secondary injection on a subscale DBN transition behaviour. The first test campaign revealed that the cavity volume did not have a significant impact on the DBN retransition NPR or side-loads generation during the descent phases. However, the presence of the cavity clearly influenced side-loads generation during transition as the side-loads were reduced by over half for the two biggest cavity volume configurations. The latter observation was attributed to the controlled and symmetric flow separation made possible by the presence of the injection slot and the cavity located downstream of the inflection region. The same behaviour was observed for the thrust jump during transition, where the magnitudes of the jumps were reduced by nearly half for the biggest cavity volume configuration.

When secondary injection was operated, several secondary mass flow rate ratios ranging from 0.011 to 0.062 were considered. The transition NPR was delayed by nearly 24% for a mass flow rate ratio of 0.025 compared to the smooth nozzle (without secondary injection slot). The retransition NPR was delayed by 20.1% for a mass flow rate ratio of 0.036 compared to the smooth nozzle. The experiments showed that the transition and the retransition NPR delay were limited, as both parameters decreased for an increasing secondary injection mass flow rate ratio once their maximum had been reached. The side-loads were decreased below 1% of the nozzle thrust during both: transition, and retransition phases using a secondary mass flow rate ratio of only 0.015. Moreover, secondary injection reduced the thrust-jump-to-thrust ratio during transition up to 2.6 percentage points and during retransition up to 3.1 percentage points for the highest secondary mass flow rate ratio compared to the smooth nozzle case. Even though dual-bell nozzles performance gain compared to a conventional nozzle is obtained at high altitude, a trade-off was achieved to determine the best secondary injection mass flow rate ratio for the present dual-bell nozzle case study.

A complete interpretation of the present results necessitates further numerical work. In addition, some further parametrical investigation and noticeably the streamwise position of the injection slot will be an interesting aspect of DBNs regime transition control.

The results presented constitute a proof of concept of the radial secondary injection on a cold flow subscale DBN model, investigations at industrial Reynolds number should demonstrate the effectiveness of the injection method on real scale rocket nozzles.

V. Acknowledgments

We would like to gratefully acknowledge the laboratory of Excellence CAPRYSSES framework and the financial support of this study from Grant No. ANR-11-LABX-0006-01 of the Investissements d'Avenir LabEx CAPRYSSES. We would also like to thank Nicolas Gouillon for his technical assistance.

References

[1] Stark, R., Génin, C., Schneider, D., and Fromm, C. "Ariane 5 Performance Optimization Using Dual-Bell Nozzle Extension." *Journal of Spacecraft and Rockets*, Vol. 53, No. 4, 2016, pp. 743–750. https://doi.org/10.2514/1.A33363.

[2] Hagemann, G., Immich, H., Nguyen, T. van, and Dumnov, G. E. "Advanced Rocket Nozzles." *Journal of Propulsion and Power*, Vol. 14, No. 5, 1998, pp. 620–634. https://doi.org/10.2514/2.5354.

[3] Walter .C, S. *The Influence of Nozzle Design on the Flight Performance of Rocket Vehicles, with an Analysis of the Results of Jet Separation*. California Institute of Technology, Pasadena, 1948.

[4] Frey, M., and Hagemann, G. "Critical Assessment of Dual-Bell Nozzles." *Journal of Propulsion and Power*, Vol. 15, No. 1, 1999, pp. 137–143. https://doi.org/10.2514/2.5402.

[5] Hagemann, G., Terhardt, M., Haeseler, D., and Frey, M. "Experimental and Analytical Design Verification of the Dual-Bell Concept." *Journal of Propulsion and Power*, Vol. 18, No. 1, 2002, pp. 116–122. https://doi.org/10.2514/2.5905.

[6] Kusaka, K., Kumakawa, A., Niino, M., Konno, A., and Atsumi, M. Experimental Study on Extendible and Dual-Bell Nozzles under High Altitude Conditions. 2000.

[7] Dumnov, G. E., Ponomaryov, N. B., and Voinov, A. L. Dual Bell Nozzles for Rocket Engines of Launch Vehicle Upper Stages and Orbital Transfer Vehicles. 1997.

[8] Ferrero, A., Conte, A., Martelli, E., Nasuti, F., and Pastrone, D. "Dual-Bell Nozzle with Fluidic Control of Transition for Space Launchers." *Acta Astronautica*, Vol. 193, 2022, pp. 130–137. https://doi.org/10.1016/j.actaastro.2021.12.048.

[9] Nürnberger-Genin, C., and Stark, R. "Flow Transition in Dual Bell Nozzles." *Shock Waves*, Vol. 19, No. 3, 2009, pp. 265–270. https://doi.org/10.1007/s00193-008-0176-4.

[10] Génin, C., and Stark, R. H. "Side Loads in Subscale Dual Bell Nozzles." *Journal of Propulsion and Power*, Vol. 27, No. 4, 2011, pp. 828–837. https://doi.org/10.2514/1.B34170.

[11] Verma, S. B., Stark, R., and Haidn, O. "Gas Density Effects on Dual-Bell Transition Behavior." *Journal of Propulsion and Power*, Vol. 28, No. 6, 2012, pp. 1315–1323. https://doi.org/10.2514/1.B34451.

[12] Zmijanovic, V., Leger, L., Sellam, M., and Chpoun, A. "Assessment of Transition Regimes in a Dual-Bell Nozzle and Possibility of Active Fluidic Control." *Aerospace Science and Technology*, Vols. 82–83, 2018, pp. 1–8. https://doi.org/10.1016/j.ast.2018.02.003.

[13] Génin, C., and Stark, R. Experimental Investigation of the Inflection Geometry on Dual Bell Nozzle Flow Behavior. 2011.

[14] Génin, C., Gernoth, A., and Stark, R. "Experimental and Numerical Study of Heat Flux in Dual Bell Nozzles." *Journal of Propulsion and Power*, Vol. 29, No. 1, 2013, pp. 21–26. https://doi.org/10.2514/1.B34479.

[15] Nasuti, F., Onofri, M., and Martelli, E. "Role of Wall Shape on the Transition in Axisymmetric Dual-Bell Nozzles." *Journal of Propulsion and Power*, Vol. 21, No. 2, 2005, pp. 243–250. https://doi.org/10.2514/1.6524.

[16] Tomita, T., Takahashi, M., Sasaki, M., and Tamura, H. Investigation on Characteristics of Conventional-Nozzle-Based Altitude Compensating Nozzles by Cold-Flow Tests. 2006.

[17] Nasuti, F., Onofri, M., and Martelli, E. Numerical Study of Transition between the Two Operating Modes of Dual-Bell Nozzles. 2002.

[18] Horn, M., and Fisher, S. *Dual-Bell Altitude Compensating Nozzles*. 1993.

[19] Verma, S. B., Stark, R., and Haidn, O. "Reynolds Number Influence on Dual-Bell Transition Phenomena." *Journal of Propulsion and Power*, Vol. 29, No. 3, 2013, pp. 602–609. https://doi.org/10.2514/1.B34734.

[20] Martelli, E., Nasuti, F., and Onofri, M. "Numerical Parametric Analysis of Dual-Bell Nozzle Flows." *AIAA Journal*, Vol. 45, No. 3, 2007, pp. 640–650. https://doi.org/10.2514/1.26690.

[21] Stark, R., and Génin, C. "Flow Separation in Rocket Nozzles under High Altitude Condition." *Shock Waves*, Vol. 27, No. 1, 2016, pp. 63–68. https://doi.org/10.1007/s00193-016-0631-6.

[22] Zmijanovic, V., Leger, L., Depussay, E., Sellam, M., and Chpoun, A. "Experimental-Numerical Parametric Investigation of a Rocket Nozzle Secondary Injection Thrust Vectoring." *Journal of Propulsion and Power*, Vol. 32, No. 1, 2016, pp. 196–213. https://doi.org/10.2514/1.B35721.

[23] Stark, R. H., and Génin, C. "Experimental Study on Rocket Nozzle Side Load Reduction." *Journal of Propulsion and Power*, Vol. 28, No. 2, 2012, pp. 307–311. https://doi.org/10.2514/1.B34253.

[24] Schneider, D., Stark, R., Génin, C., Oschwald, M., and Kostyrkin, K. "Active Control of Dual-Bell Nozzle Operation Mode Transition by Film Cooling and Mixture Ratio Variation." *Journal of Propulsion and Power*, Vol. 36, No. 1, 2019, pp. 47–58. https://doi.org/10.2514/1.B37299.

[25] Proshchanka, D., Yonezawa, K., Koga, H., Tsujimoto, Y., Kimura, T., and Yokota, K. "Control of Operation Mode Transition in Dual-Bell Nozzles with Film Cooling." *Journal of Propulsion and Power*, Vol. 28, No. 3, 2012, pp. 517–529. https://doi.org/10.2514/1.B34202.

[26] Martelli, E., Nasuti, F., and Onofri, M. "Numerical Analysis of Film Cooling in Advanced Rocket Nozzles." *AIAA Journal*, Vol. 47, No. 11, 2009, pp. 2558–2566. https://doi.org/10.2514/1.39217.

[27] Léger, L., Zmijanovic, V., Sellam, M., and Chpoun, A. "Controlled Flow Regime Transition in a Dual Bell Nozzle by Secondary Radial Injection." *Experiments in Fluids*, Vol. 61, No. 12, 2020. https://doi.org/10.1007/s00348-020-03086-3.

[28] Léger, L., Zmijanovic, V., Sellam, M., and Chpoun, A. "Experimental Investigation of Forced Flow Regime Transition in a Dual Bell Nozzle by Secondary Fluidic Injection." *International Journal of Heat and Fluid Flow*, Vol. 89, 2021. https://doi.org/10.1016/j.ijheatfluidflow.2021.108818.